Received: 2 October 2019 | Revised: 8 December 2019 | Accepted: 10 January 2020

DOI: 10.1002/joc.6481

RESEARCH ARTICLE

International Journal of Climatology | RMetS

Improving the dynamical seasonal prediction of western Pacific warm pool sea surface temperatures using a physical–empirical model

Ping Chen[1] | **Bo Sun**[1,2,3]

[1]Collaborative Innovation Center on Forecast and Evaluation of Meteorological Disasters/Key Laboratory of Meteorological Disaster, Ministry of Education, Nanjing University of Information Science and Technology, Nanjing, China

[2]Nansen-Zhu International Research Centre, Institute of Atmospheric Physics, Chinese Academy of Sciences, Beijing, China

[3]Southern Marine Science and Engineering Guangdong Laboratory (Zhuhai), Zhuhai, China

Correspondence
Bo Sun, Collaborative Innovation Center on Forecast and Evaluation of Meteorological Disasters/Key Laboratory of Meteorological Disaster, Ministry of Education, Nanjing University of Information Science and Technology, Nanjing 210044, China.
Email: sunb@nuist.edu.cn

Funding information
Jiangsu Innovation and Entrepreneurship Team; National Natural Science Foundation of China, Grant/Award Numbers: 41421004, 41805047; Science and Technology Innovation Project for Overseas Talents of Nanjing, Grant/Award Number: R2018LZ02; Scientific Research Foundation of Key Laboratory of Meteorological Disaster (KLME), Ministry of Education, Grant/Award Number: KLME201803

Abstract

The western Pacific warm pool (WPWP) has a profound impact on the global climate. In this study, the forecast skill of ENSEMBLES model for predicting the WPWP sea surface temperature (SST) for the period 1960–2006 is evaluated, where a WPWP index (WPWPI) is defined to represent the interannual variability of WPWP SST. The result indicates that the ENSEMBLES exhibit a poor skill in predicting the WPWPI during January–April (2- to 5-month forecasts starting on November 1). To improve the ENSEMBLES-predicted WPWP SSTs during January–April, a physical–empirical (PE) model is developed based on two predictors, using the year-to-year increment method and the linear regression method. The two predictors include the ENSEMBLES-predicted sea level pressure during January and the observed northern tropical Atlantic SSTs during the preceding August. The mechanisms associated with the two predictors are illuminated. The 1-year-out cross-validation and the independent hindcast indicate that this PE model may notably improve the WPWPI prediction of ENSEMBLES, with a correlation coefficient (CC) above 0.6 between the PE-model-predicted WPWPI and the observed WPWPI during January–April. The physical mechanisms expounded in this study and the PE model utilized in this study can be considered to improve the prediction of WPWP SST of numerical models in the future.

KEYWORDS

ENSEMBLES, physical–empirical model, prediction, warm pool, year-to-year increment approach

1 | INTRODUCTION

The western Pacific warm pool (WPWP) is a crucial component of tropical oceans. It has been identified as both the warmest portion of the heat reservoir and the hottest portion of the firebox where a huge amount of precipitation-induced latent-heat release is accumulated due to the maximum annual precipitation (Chen *et al.*, 2004). The importance of WPWP for global climate has been widely recognized (Wang and Xie, 1998; Clement *et al.*, 2005; Wang and Mehta, 2008; De Deckker, 2016; Hu *et al.*, 2017; Li *et al.*, 2017). For instance, the sea surface temperatures (SSTs) in WPWP reflect the variability of El Niño-South Oscillation (ENSO), which is the dominant influential factor of interannual variability of global climate (Matsuura and Iizuka, 2000; D'Arrigo *et al.*, 2006; Hu *et al.*, 2017; Shen *et al.*, 2019). The WPWP SSTs also exert important influences on the East Asian monsoon (Nitta, 1986, 1987; Huang, 1992; Matsuura and Iizuka, 2000; Sun *et al.*, 2016), the greenhouse effect (Rajeevan and McPhaden, 2004; Ruiz *et al.*, 2005), and the precipitation along the coast of China (Li and Zhou, 1999). Thus, the evaluation of forecast skill for WPWP SSTs as well as the improvement of the forecast skill for WPWP SSTs is a critical issue for the prediction of climate variability.

Many efforts have been done to examine the predictive skill of dynamical and statistical models for the tropical SSTs (Tangang *et al.*, 1997; Berliner *et al.*, 2000; Saha *et al.*, 2006; Wu *et al.*, 2006; Weisheimer *et al.*, 2009; Stockdale *et al.*, 2011). Specifically, (a) dynamical models showed anomaly correlation skill of ~0.5 up to 12 months ahead for eastern Pacific SST such as the Niño3 or Niño3.4 SST (Saha *et al.*, 2006; Weisheimer *et al.*, 2009; Stockdale *et al.*, 2011); (b) statistical model were viable for ENSO forecasting even at longer lead times of 9–12 months (Tangang *et al.*, 1997; Wu *et al.*, 2006); Kang and Kug (2000) also developed an El Niño prediction model, which can predict the eastern Pacific and central Pacific for up to 12 months. However, most of the above studies focused on the predictive skill of dynamical and statistical models for the eastern tropical Pacific SSTs. Less effort has been done to examine and improve the predictive skill for the WPWP SSTs.

Generally, two approaches can be used to improve numerical-model-forecasted products. The first approach is to improve the numerical model via tuning the dynamic processes and parameterization and resolution of the numerical model (Gao *et al.*, 2008, 2018; Gao and Giorgi, 2017; Sun *et al.*, 2018). For instance, Weisheimer *et al.* (2009) improved models used in ENSEMBLES in all aspects: in physical parameterizations, in resolution and in the initialization. Doblas-Reyes *et al.* (2009) compared three models obtained from ENSEMBLES by setting up perturbed parameter and stochastic physics techniques. The other approach is on the basis of numerical model forecast, to establish a physical–empirical (PE) model containing several predictors and a predictand to improve the original forecast of numerical model, where the underlying physical mechanism between the predictors and the predictand has to be well understood (Huang *et al.*, 2014; Tian and Fan, 2014; Fan *et al.*, 2016; Bi *et al.*, 2018; Tian *et al.*, 2018; Zhang *et al.*, 2019a). For instance, Huang *et al.* (2014) developed a physical–empirical model to improve the ability to predict the interannual variability of the summer rainfall over the Yangtze River valley with two predictors of Asian–Pacific Oscillation and SST anomaly over the Atlantic. Zhang *et al.* (2019b) established a physical–empirical model to improve the prediction of Antarctic Oscillation Index (AOI), with two predictors including concurrent spring SSTs forecasted by NCEP Climate Forecast System Version 2 (CFSv2) and observed preceding autumn sea ice.

Thus, this study aims to examine the predictive skill of the ENSEMBLES model for the WPWP SSTs and to improve the ENSEMBLES prediction of WPWP SSTs using a physical–empirical model, which is established based on an understanding of the mechanisms for the interaction between the WPWP SSTs and the predictors for WPWP SSTs.

The structure of this article is as follows. Section 2 introduces the data and methods applied in this study. The predictive skill of the ENSEMBLES with regard to WPWP SST is discussed in section 3. In section 4, the two predictors applied to predict the WPWP SST are introduced first, then the PE model is established and adopted to improve the prediction of WPWP SST in ENSEMBLES. Finally, section 5 provides some discussions and conclusions.

2 | DATA AND METHODS

2.1 | Data

ENSEMBLES is a comprehensive project funded by the European Union to establish a climate change ensemble forecasting system based on the most advanced, high-resolution, global and regional Earth system models developed in Europe, and to validate European data through quality control, high-resolution grids (Doblas-Reyes *et al.*, 2009). The multi-model ensemble for seasonal-to-annual forecasts comprises of global coupled atmosphere–ocean climate models from the UK Met Office (UKMO), Météo France (MF), the European Centre for Medium-Range Weather Forecasts (ECMWF), the Leibniz Institute of Marine Sciences at Kiel University (IFM-GEOMAR), the Euro-Mediterranean Centre for Climate Change (CMCC-INGV) in Bologna, and the Hadley Centre Coupled Model version 3 (HadCM3), with hindcast data for the period of 1960–2005. Each year has 7-month-long seasonal forecasts starting on the first of February, May, August and November. In addition, the November forecasts from all models except for CMCC-INGV were extended to 14-month-long annual forecast. In this study, the 14-month long annual forecasts starting on the first of November are utilized. Since the HadCM3 model does not have the hindcast data of SLP, the multi-model ensemble-mean

(MME) of SLP does not include the HadCM3 model. In addition, equal weights are applied to all models when computing the multi-model ensemble-mean (MME) of ENSEMBLES.

The reanalysis data included vertical velocity (ω), surface wind, 850-hPa wind and SLP data are derived from the monthly reanalysis data of National Centers for Environmental Prediction (NCEP) and National Center for Atmospheric Research (NCAR), which has a resolution of 2.5°× 2.5° (Kalnay *et al.*, 1996). The ω is at levels of 1,000, 925, 850, 700, 600, 500, 400, 300, 250, 200, 150 and 100-hPa. Observation data of SST is derived from the Met Office Hadley Center, which has a resolution of 1° × 1° (Rayner *et al.*, 2003). Particularly, the net long-wave radiation fluxes, net shortwave radiation fluxes, latent heat net fluxes and sensible heat net fluxes derived from NCEP/NCAR are on T62 Gaussian grids (192 × 94).

2.2 | Methods

In this study, the temporal correlation coefficient (CC) and the root-mean-square error (RMSE) are adopted to evaluate the prediction skill of the ENSEMBLES multi-model. Additionally, the RMSE does not discriminate between systematic and random errors of the model, thus an alpha index (AI) proposed by Koh and Ng (2009) is applied in this study to evaluate random errors of the model. The *AI* is given by:

$$\mathrm{AI}=1-2\frac{\mathrm{cov}(F,O)}{\mathrm{var}(F)+\mathrm{var}(O)}=\frac{\sum_{i=1}^{N}\left(F_i-\bar{F}-O_i-\bar{O}\right)^2}{\sum_{i=1}^{N}\left(F_i-\bar{F}\right)^2+\sum_{i=1}^{N}\left(O_i-\bar{O}\right)^2}$$

where F is the time series of hindcast and O is the time series of observations; cov(F,O) is the covariance between the forecast and observation; var(F) and var(O) are the variance of forecast and observation, respectively; N is the length of time series; the overbar denotes climate mean. The AI ranges from 0 to 2. Thus, in the case of $F_i - \bar{F} \approx O_i - \bar{O}$, AI approaching 0, which denotes a small random error and a better prediction skill; in the case of *cov* (F,O) ≈ 0, AI approaching 1, which denotes a large random error and poor agreement between the prediction and observation; in the case of $F_i - \bar{F} \approx -(O_i - \bar{O})$, AI approaching 2, which indicates that the random error is small and the difference between forecast value and the observation is large. For a good numerical-model forecast, the AI should be less than 1.

In this study, we establish a PE model to improve the original forecast of ENSEMBLES. First, the predictors of the predictand are determined, and then the PE model is established by using the concurrent predictor predicted by model and the previous information in the observation data.

Compared to the traditional prediction models which aim at predicting the anomalies of a variable, a year-to-year increment approach was applied to develop the PE model. The year-to-year increment approach proposed by Fan *et al.* (2008) based on Wang *et al.* (2000) treats the year-to-year increment (DY, the difference in a variable between current year and previous year) of a variable as the predictand, produces the final predicted variable by adding the predicted DY of the variable to the observed value from the previous year. Results have suggested that the year-to-year increment approach can obviously improve the prediction of East Asian winter monsoon (Tian *et al.*, 2018), AOI (Zhang *et al.*, 2019b), and the winter North Atlantic Oscillation (Fan *et al.*, 2016). Huang *et al.* (2014) pointed out that adding model-predicted DY of the North Pacific tropospheric temperature index (PI) to observed PI from the previous year can improve the model's prediction of PI. Specially, the year-to-year increment approach is mainly used in the context of the quasi-biennial oscillation of the variables of the tropospheric climate, such as the East Asian monsoon, ENSO and other climatic factors. It is not difficult to understand why the year-to-year increment approach is useful for better prediction. Specifically, if Y_{i} represents the variable in the current year and Y_{i-1} represents the variable in the previous year, then $Y_{\mathrm{i}} = C + d_{\mathrm{i}}$ and $Y_{i-1} = -C + d_{\mathrm{i}-1}$, where C represents the anomaly of the variable, and where d_{i} and d_{i-1} represent a disturbance in C. After the disturbance is ignored, the climatological mean is 0, then the climatic anomaly of Y_{i} is $Y_{\mathrm{i}} - 0 = C + d_{\mathrm{i}} \approx C$ and the year-to-year increment of Y is $\mathrm{DY}_{\mathrm{i}} = Y_{\mathrm{i}} - Y_{i-1} \approx 2\mathrm{C}$. If DY is considered as the predicand, then the amplitude of DY is twice the amplitude of Y. Thus, using the year-to-year increment prediction approach could largely amplify the prediction signals.

The PE model's predictive capability is assessed using 1-year-out cross-validation (Michaelsen, 1987) and independent hindcast. The 1-year-out cross-validation method predicts the predictand in the specific year with a model built by the sample of leaving this specific year out. Independent hindcast divided the database in two periods, one applied for training period of 1963–1984 and another period of 1985–2006 for verification. The statistical significance of correlation coefficients (CCs) is assessed using the Student's *t*-test.

In section 4.1.2, the ENSO signal is removed by the following formula (Li *et al.*, 2006):

$$\mathrm{SST}^* = \mathrm{SST}-(\text{Niño3.4} \times a+b)$$

$$a = \mathrm{cov}(\text{Niño3.4},\mathrm{SST})/\mathrm{var}(\text{Niño3.4})$$

$$b = \mathrm{avg}(\mathrm{SST})-a \times \mathrm{avg}(\text{Niño3.4})$$

where SST* is the SST field after ENSO signal is removed; SST is the original SST field; cov(Niño3.4, SST) is the covariance between the Niño3.4 index and SST; var(Niño3.4) is the variance of Niño3.4 index; avg(SST) is the average of SST filed; avg(Niño3.4) is the average of Niño3.4 index.

Considering that this study focuses on the interannual variability, the linear trends in the data during 1960–2006 are removed before all computations.

3 | THE FORECAST SKILL OF ENSEMBLES FOR THE WPWP SST

In the previous study, there are many definitions for WPWP using different isotherms as its boundary for different purposes (Graham *et al*., 1987; Webster and Lukas, 1992; Picaut *et al*., 1996; Ridout and Reynolds, 1998; Wang *et al*., 2010; Gan and Wu, 2012). For instance, Gan and Wu (2012) utilized an isotherm of 28°C as the boundary of WPWP. Ridout and Reynolds (1998) used the isotherm of 29°C to identify the WPWP. To examine the model's predictive ability for the WPWP SST and to avoid the influence of regional changes caused by the selection of specified isotherm on the score of forecast skill, this study follows Zhan *et al*. (2013) and defines the WPWP index (WPWPI) by the SST averaged over the region within 0°–16°N and 125°E–165°E.

Figure 1 shows the predictive skill scores of the multi-model ENSEMBLES for WPWP SST from 1960 to 2006 based on different metrics. The CCs between the observation and the EMSEMBLES MME for the WPWPI decrease rapidly towards a low level after 2-month forecasts, with a CC below 0.4 (significant below the 99% confidence level) for most models (Figure 1a). Specifically, the HadCM3 model has a relatively higher forecast

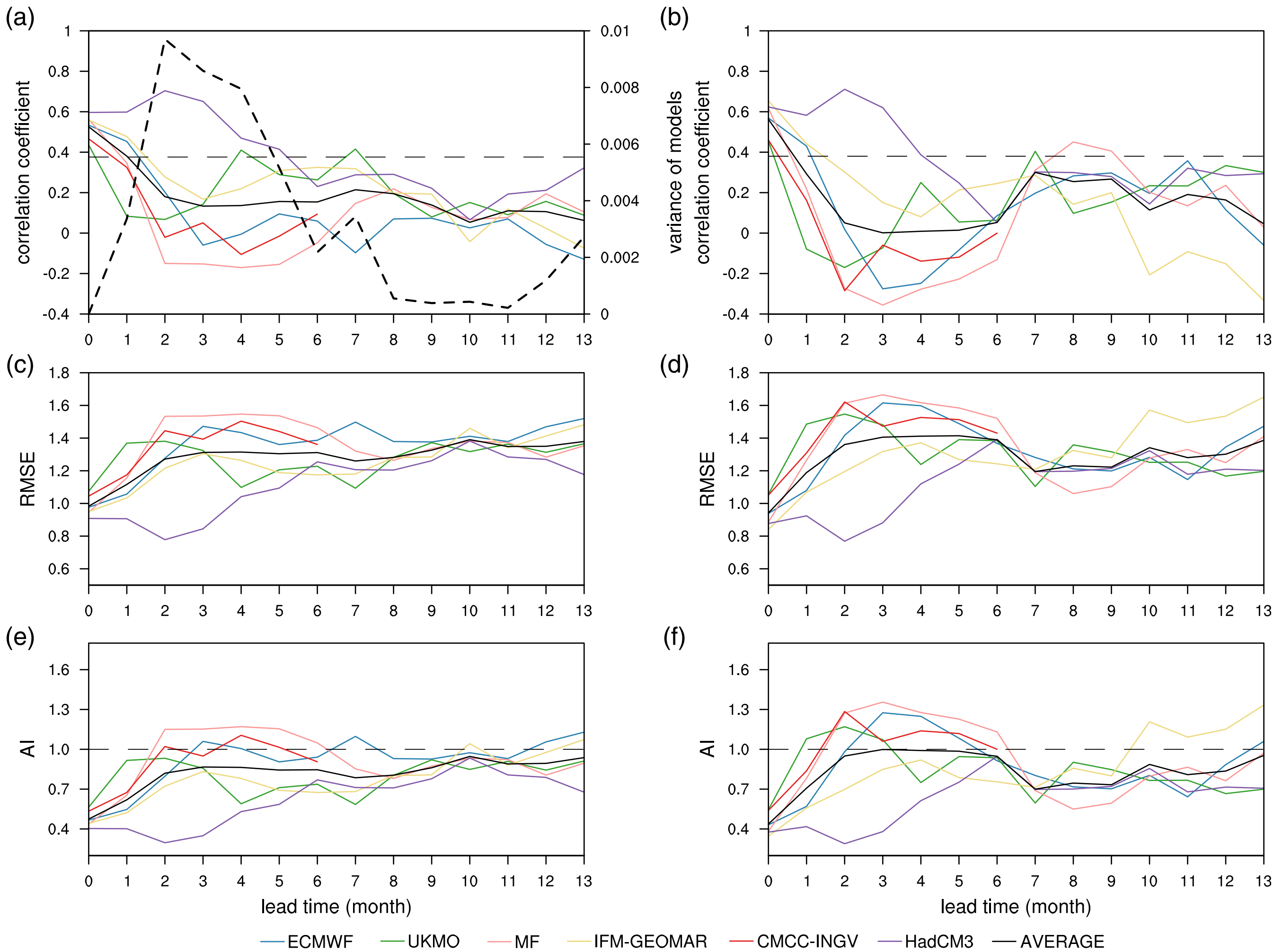

FIGURE 1 (a–b) Correlation coefficients, (c–d) RMSEs and (e–f) AIs between the ENSEMBLES multi-models and the observation for WPWPI (left panel) and DY_WPWPI (right panel) starting on November 1st for the period 1960–2005. The lead time 0 in the *X*-axis refers to November. Colour code: Blue, ECMWF; green, UKMO; pink, MF; yellow, IFM-GEOMAR; red, CMCC-INGV; purple, HadCM3; black, the MME. In (a) and (b), the horizontal dashed line indicates the 99% confidence level based on the Student's *t*-test. In (a), thick black dashed line indicates the variance of multi-models

skill score for WPWPI than other models, which has a CC with the observation higher than 0.4 (significant at the 99% confidence level) within the 5-month forecasts. The CCs between the observed and forecasted DY of WPWPI (DY_WPWPI) show similar features (Figure 1b). Correspondingly, for the MME and for most models, the RMSEs between the observation and forecasts (Figure 1c) and the AIs (Figure 1e) increase towards a high level after the 2-month forecast, indicating a notably decreased forecast skill for most models after the 2-month forecast. Moreover, the CCs, RMSEs, and AIs for different models exhibit a noticeable variance after the 2-month forecast, suggesting a large uncertainty of the model forecasts of WPWPI. The 2-month forecast refers to the January forecast starting on first of November. Thus, the forecast for WPWPI for the months during January–April needs to be improved.

4 | IMPROVEMENT OF WPWP SST PREDICTIVE SKILL-BASED ON THE PE MODEL

Wavelet analyses are computed for the January–April WPWPI during 1960–2006. The results indicate that the monthly WPWPI during January–April has a significant 2- to 6-year period (Figure 2). Thus, the year-to-year increment method can be utilized to establish the PE model, which may enlarge the signal of interannual variability of WPWPI and hence be conducive to the prediction of WPWPI. Considering that the WPWP SST is affected by regional air–sea interaction (Da Silva *et al.*, 1994; Wu *et al.*, 2006) and is teleconnected with the air-sea interaction over Atlantic (Enfield *et al.*, 2006; Ham *et al.*, 2013), two predictors are utilized to establish the PE model for improving the forecast skill of WPWPI, which are the regional SLPs and the northern tropical Atlantic (NTA) SSTs, respectively.

4.1 | Predictors and associated mechanisms

4.1.1 | Regional SLP over WPWP

Previous studies indicate that the regional air–sea interaction over WPWP may exert an impact on the WPWP SSTs (Sun *et al.*, 2017). An anomalous depression or subsidence over the WPWP may induce Walker circulation anomalies, surface winds anomalies, cloud anomalies and radiation fluxes anomalies, resulting in SST anomalies (Madden and Julian, 1994; Knaff, 1997; Wang and Enfield, 2001; Druyan and Hastenrath, 2002; Zelinka and Hartmann, 2010; Soden and Vecchi, 2011). These SST anomalies may persist in the following months due to the low-frequency variation of SSTs (Luksch and von Storch, 1992). Thus, regional climate variables associated with the air–sea interaction over the WPWP during January or preceding January could be considered potential predictors for the WPWPI during January–April.

One of the regional potential predictors of WPWP SST is the SLP over WPWP. As shown in Figure 3, the lead–lag CCs between the DY_SLP during January and the DY_WPWPI during January–April indicate that anomalous low regional DY_SLP during January is generally associated with positive DY_WPWPI during January–April, suggesting that the regional SLP during January can be used as a predictor of WPWPI during January–April to establish the PE model from a statistical perspective.

However, the question is: how the regional SLP during January influences the air–sea interaction and hence influences the WPWP SSTs during January–April? To answer this question, the climate anomalies associated with the anomalous regional SLP over the WPWP are examined, where a SLP index (SLPI) is defined as the areal mean SLP over the region within 10°S–20°N, 120°–165°E. Figure 4 shows the 850-hPa ω anomalies during January–April regressed on the SLPI during January. It can be seen that negative ω anomalies occur over the WPWP during January concurrent with an anomalous depression (Figure 4a). The enhanced vertical ascending motion over western tropical Pacific induces a strengthened Walker circulation over the tropical Pacific, which is characterized by ascending anomalies over the tropical Pacific within 110°–165°E and descending anomalies over the tropical Pacific within 165°–90°W (Figure 4b). This strengthened Walker circulation may lead to increase near-surface easterly winds over the tropical Pacific (Figure 5a), inducing a large amount of warmer seawater in the central equatorial Pacific to be transported to the western Pacific (Kucharski *et al.*, 2011). The convergence of the surface waters in the western Pacific results in increased WPWP SSTs (Figure 5b). At the same time, the western boundary of the WPWP is composed of sporadic islands, which also weakens the boundary upwelling and is conducive to the increase of the WPWP SSTs (Wu, 1993).

In turn, the increased WPWP SSTs may provide a boundary condition favouring the strong upward atmospheric motions and convection over the WPWP, which may enhance the easterly winds over tropical central Pacific and then strengthen the cold anomaly in the central-eastern equatorial Pacific through increased upwelling. The Bjerknes feedback may amplify the coupling of the temperature gradient of east–west sea surface

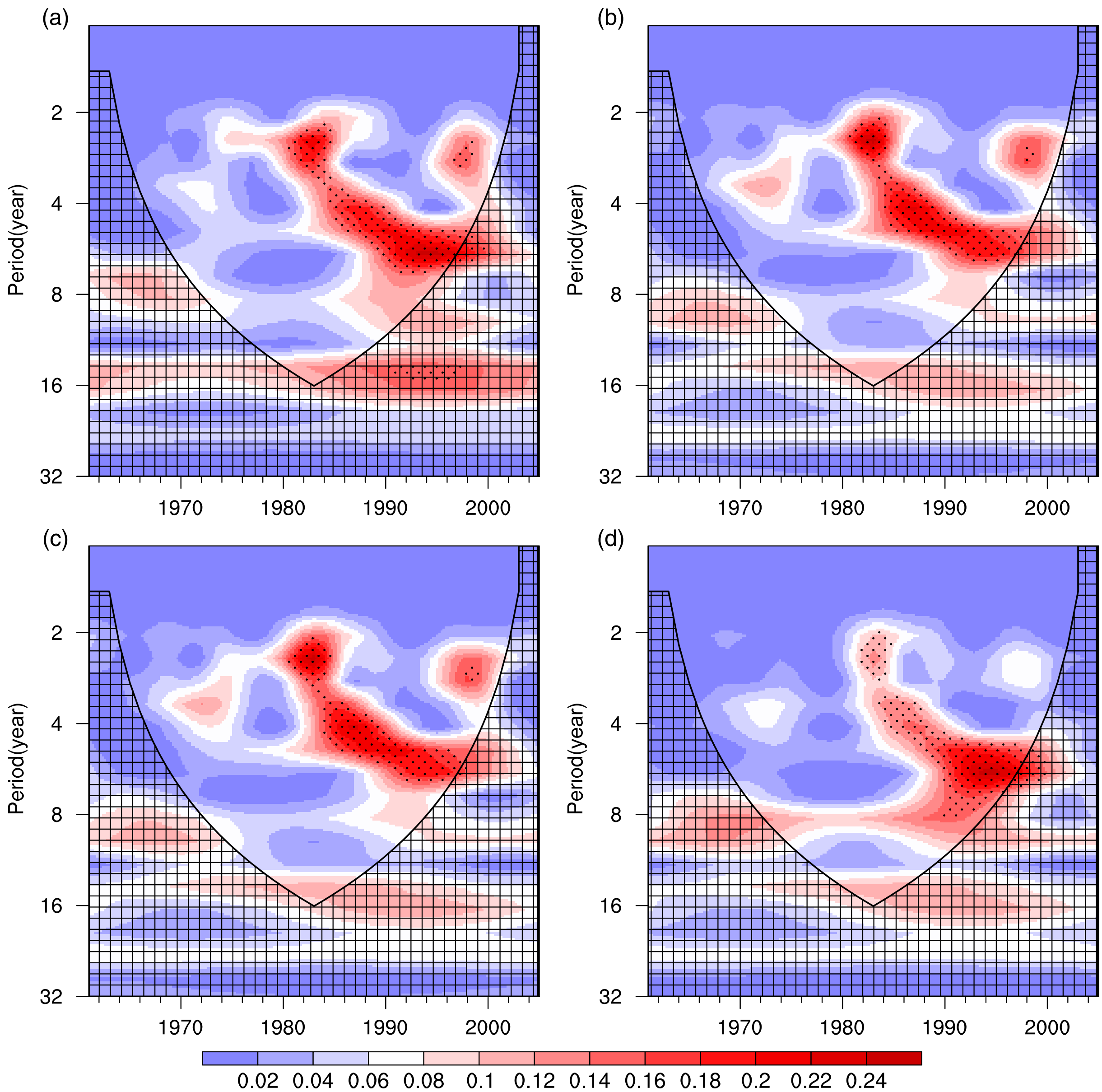

FIGURE 2 Wavelet analyses of the WPWPI during (a) January, (b) February, (c) march and (d) April for the period 1961–2006. Dotted regions indicate significant variability at the 90% confidence level estimated by a red noise process, and the parabola indicates the "cone of influence"

and the strengthened Walker Circulation (Figure 4e,h,k and 5c,e,g; Bjerknes, 1969). This positive feedback can persistently warm WPWP SST during January–April (Figure 5b,d,f,h). However, the Pacific SST also has its own variability, not completely controlled by the Walker circulation, and there are many factors that inhibit its warming (Kitoh *et al.*, 1999). For example, the more convective cloud associated with increased convective activity reduce the incoming solar radiation, which cool the SST, so this positive feedback only affects the seasonal changes of the SST.

It should be noted that previous studies suggested that the regional SLP and convection may influence the WPWP SSTs via affecting the surface heat budget, including the net long-wave radiation, net shortwave radiation, latent heat net fluxes and sensible heat net fluxes (Cronin and McPhaden, 1997; Shinoda and Hendon, 1998; Huo and Xiao, 2017). However, our result shows that although net long-wave radiation and sensible and latent heat fluxes are responsible for the positive net heat fluxes anomaly into the ocean, which warms up SST, while the net shortwave radiation counter-acts the other three radiation factors, the correlation coefficients between WPWP net surface heat fluxes and the WPWP SST anomalies are not significant in any lag/lead month (Figure 6a). In contrast, Figure 6b shows that the maximum negative

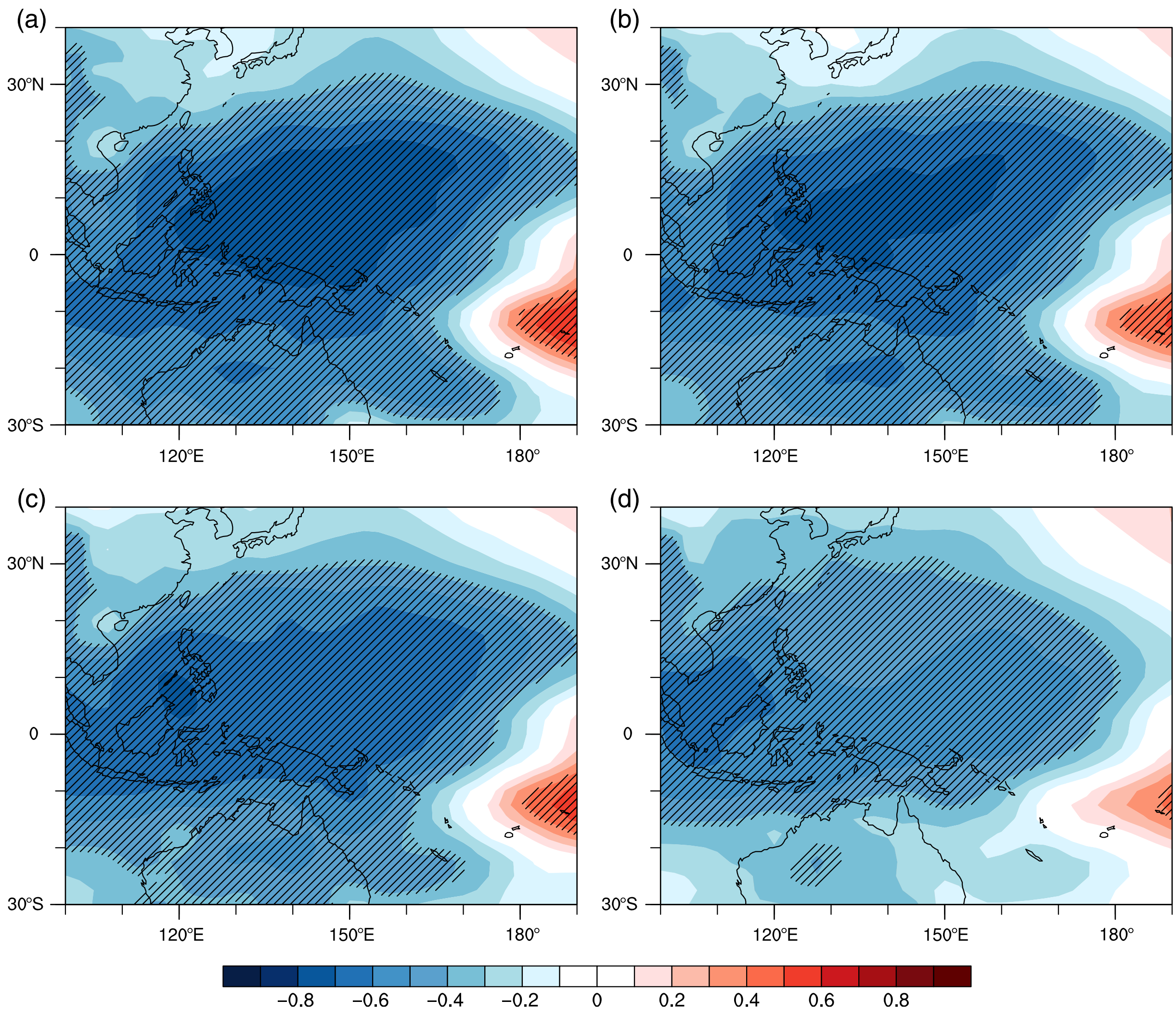

FIGURE 3 Correlation coefficients between the observed January DY of SLP and observed DY_WPWPI during (a) January, (b) February, (c) March and (d) April. Slashed areas indicate statistical significance at the 99% confidence level based on the Student's *t*-test

correlation between the WPWP SSTs and the near-surface zonal wind averaged over the tropical Pacific (10°S–5°N, 160°E–150°W) occurs when the lag month is zero, with a correlation coefficient of −0.57, which is above the 99% significance level. The lead–lag CCs are still significant when the WPWP SSTs lead/lag the near-surface zonal wind by 5 months. The above results suggest that the regional SLP over the WPWP and the associated near-surface zonal wind anomalies over the tropical Pacific are more important factors for inducing the anomalous WPWP SSTs during January–April than the surface heat budget.

Furthermore, the SLP over the WPWP region is better predicted than WPWP SST, because the SST anomalies in the western Pacific are smaller than the SST anomalies in the eastern Pacific, whereas the SLP anomalies in the east and west are not much different (Xue and Leetmaa, 2000). As depicted in Figure 7, the ENSEMBLES MME shows a better skill for predicting the SLPI than WPWPI for lead-times of 2–5 months. The lead times of 2–5 months refer to the forecast during January–April starting on November 1. Specifically, for the 2- to 5-month forecasted WPWPI, the CCs between the observed WPWPI and the forecasted WPWPI are approximately 0.2, which are below the 90% significance level (Figure 7a); whereas the CCs between the observed SLPI and the forecasted SLPI are approximately 0.75, which are above the 99% significance level (Figure 7a). These results indicate that the ENSEMBLES MME has a better skill for predicting the SLP than for predicting the SSTs over the WPWP regarding the 2- to 5-month forecast. As for the DY, the CCs between the observed DY_WPWPI and the forecasted DY_WPWPI are approximately 0.0 for the 2- to 5-month forecast; in contrast, the CCs between

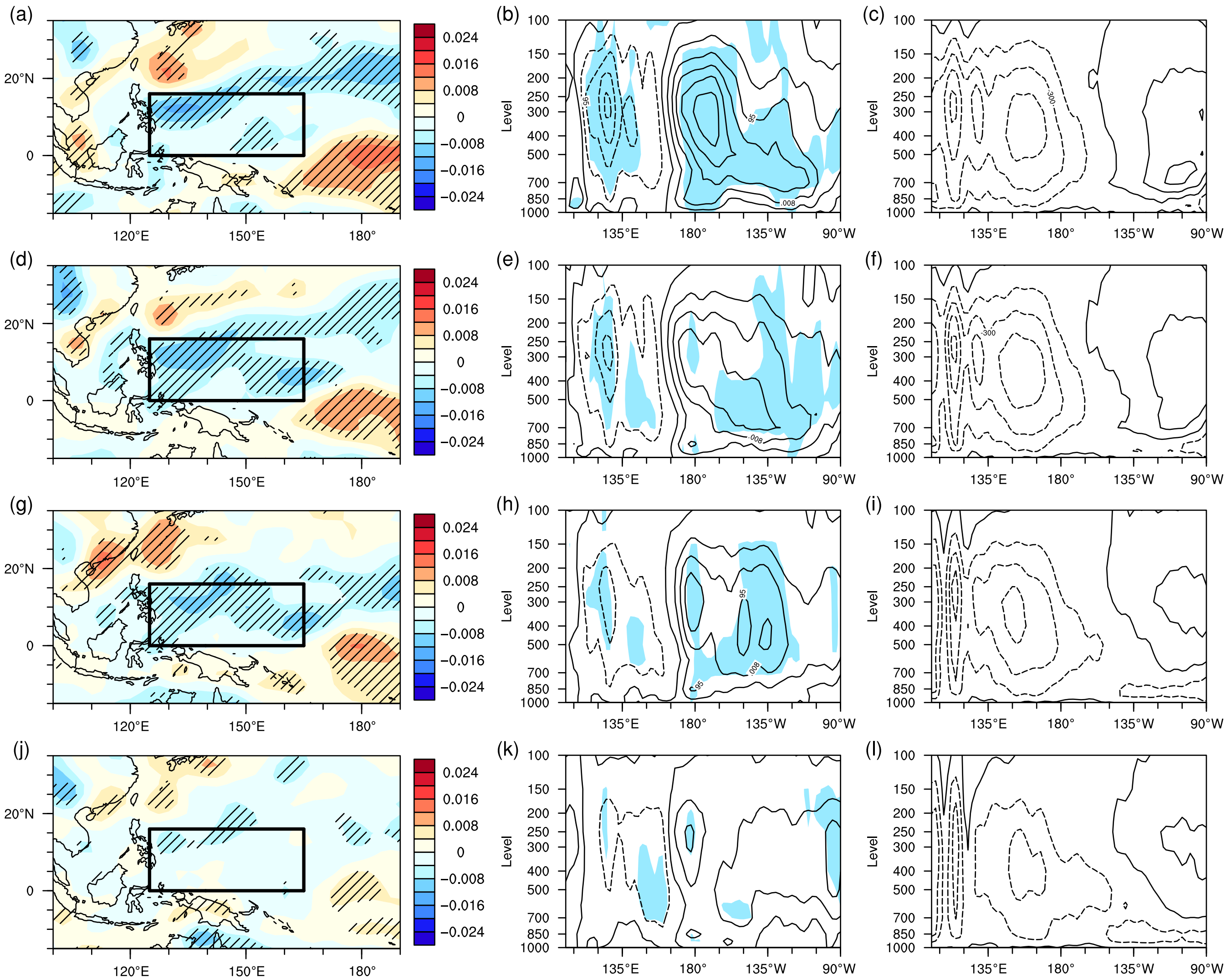

FIGURE 4 Anomalies of observed 850-hPa ω (unit: 10^{-3} Pa s^{-1}; left panel) and meridional averaged ω within 5°S–5°N (unit: 10^{-3} Pa s^{-1}) (middle panel) during (a–b) January, (d–e) February, (g–h) March and (j–k) April regressed on the standardized time series of observed January SLPI for 1960–2006. Climatology of meridional averaged ω within 5°S–5°N (right panel) during (c) January, (f) February, (i) March and (l) April. Slashed areas in (a, d, g, j) and shaded areas in (b, e, h, k) indicate statistical significance at the 95% confidence level based on the Student's *t*-test. The black curvilinear rectangles in (a, d, g, j) represent the region of WPWP

the observed DY_SLPI and the forecasted DY_SLPI are approximately 0.8 for the 2- to 5-month forecast, which are above the 99% confidence level (Figure 7b). In addition, as shown in Figure 7c, the RMSEs for the forecasted SLPI are notably smaller than the RMSEs for the forecasted WPWPI regarding the 2- to 5-month forecast, indicating a better predictive skill for the SLPI than for the WPWPI. At the same time, the ENSEMBLES-predicted January SLP is significantly correlated with the observed WPWPI during January–April. The 2- to 5-month forecast we mentioned above refers to the forecast during January–April starting on November 1. Thus, the January SLPI forecasted by the ENSEMBLES MME can be used as a predictor for establishing the PE model of predicting WPWPI for January–April.

4.1.2 | Northern tropical Atlantic SSTs

Previous studies demonstrate that SST anomalies over NTA area may exert regional air–sea interaction and further produce teleconnections over the tropical ocean (Jansen *et al.*, 2009; Frauen and Dommenget, 2012; Kucharski *et al.*, 2016; Sun *et al.*, 2017). In particular, some studies documented the impact of the Atlantic Multidecadal Oscillation (AMO) on the Pacific SSTs (Enfield *et al.*, 2006;

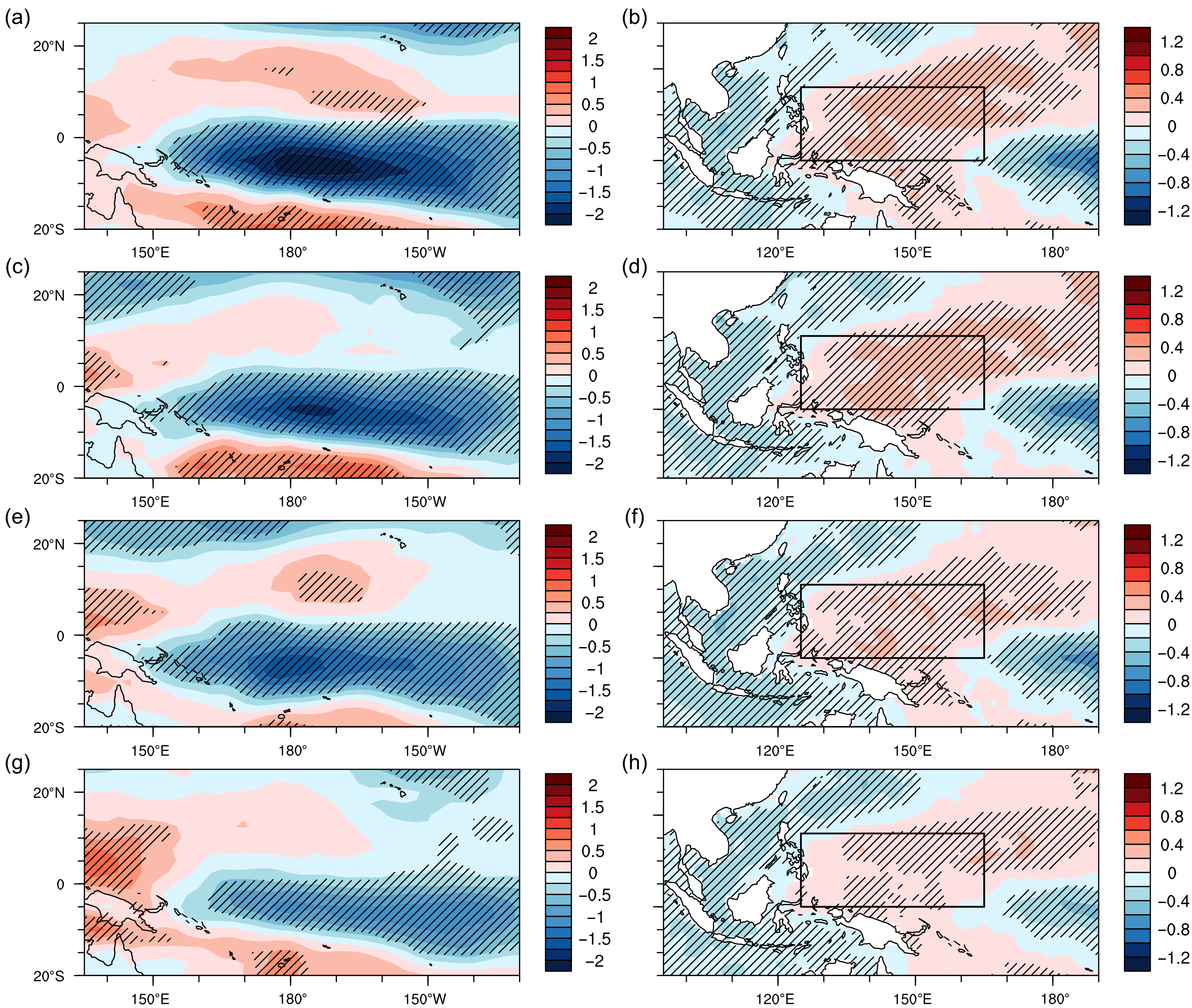

FIGURE 5 Observed surface zonal wind (unit: m s^{-1}; left panel) and SST (unit: °C; right panel) during (a–b) January, (c–d) February, (e–f) March and (g–h) April regressed on the standardized time series of observed January SLPI for 1960–2006. Slashed areas indicate statistical significance at the 95% confidence level based on the Student's *t*-test. The black curvilinear rectangles in (b, d, f, h) represent the region of WPWP

Timmermann *et al.*, 2007; Zhang and Delworth, 2007). It is suggested that the warming of NTA SST may induce westerly wind anomalies over the eastern Pacific as Rossby waves and easterly wind anomalies over the Indo-western Pacific as Kelvin waves and these wind anomalies induce eastern Pacific cooling and Indo-western Pacific warming (Ham *et al.*, 2013; Li *et al.*, 2016; Sun *et al.*, 2017). Considering the aforementioned teleconnection between the NTA SSTs and the tropical Pacific SSTs, the NTA SSTs could be considered a potential predictor for the WPWPI during January–April.

The relationship between the observed monthly WPWPI during January–April and the monthly NTA SSTs during preceding boreal summer and autumn is examined. The results indicate a significant correlation between the preceding August NTA SSTs and the WPWPI during January–April. Figure 8 depicts the correlation coefficients between the DY_SST of preceding August and the monthly DY_WPWPIs during January–April. It can be seen that the DY_WPWPI during January–April are all significantly correlated with the NTA SSTs (areal mean SST anomalies within 0°–15°N, 90°W–20°E) during the preceding August. Thus, from a statistical perspective, the NTA SSTs during the preceding August can be considered a predictor to establish the PE model for predicting the WPWP SSTs during January–April.

To illustrate the mechanism how the preceding NTA SSTs impact the WPWP SSTs during January–April, a

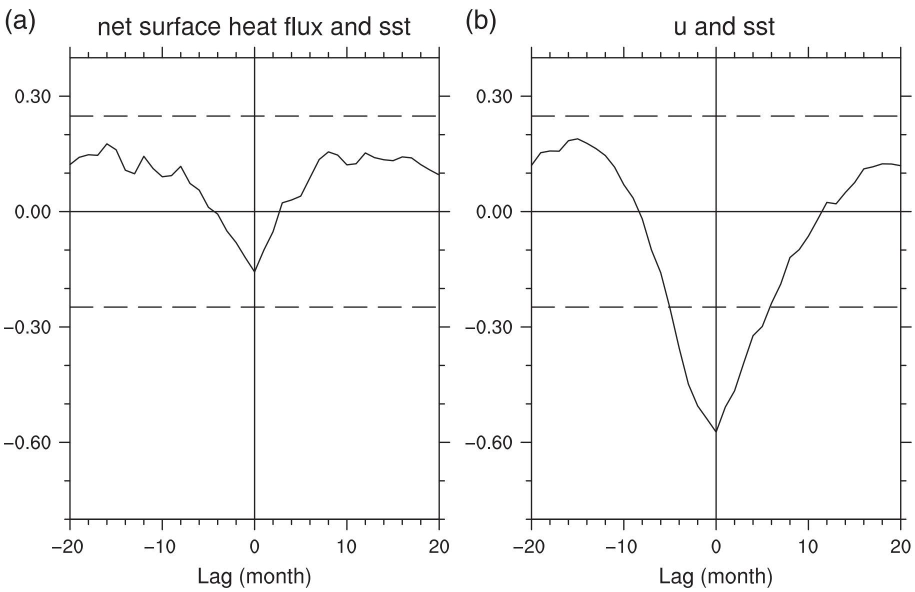

FIGURE 6 Lagged cross-correlation coefficients between observed January WPWPI and (a) the net surface heat fluxes (unit: W m^{-2}), (b) the zonal wind at 10 M (unit: m s^{-1}). The horizontal dashed lines represent 90% significance level based on the Student's *t*-test. The net surface heat fluxes are calculated as the regionally averaged net surface heat fluxes over WPWP area (positive out of the ocean). The zonal wind is calculated as the regionally averaged zonal wind over 10°S–5°N, 160°E–150°W

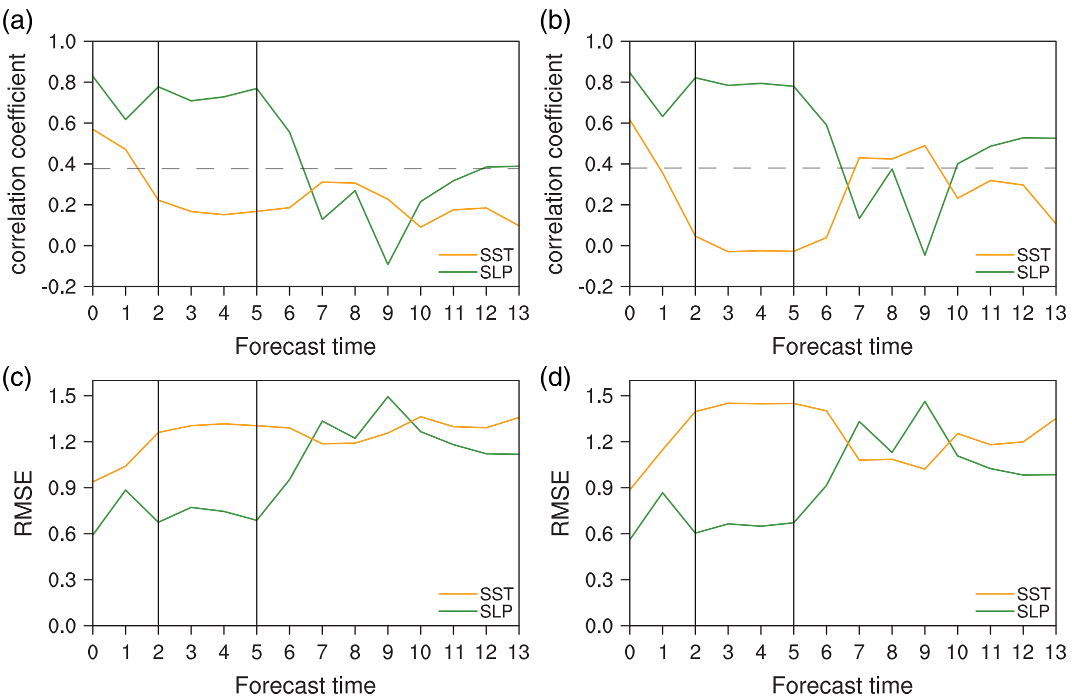

FIGURE 7 (a, b) Correlation coefficients and (c, d) RMSEs between ENSEMBLES MME and the observation for SLPI and WPWPI (left panel), DY_SLPI and DY_WPWPI (right panel) starting on first of November for the period 1960–2005. The horizontal dashed line in (a, b) indicates the 99% confidence level based on the Student's *t*-test

northern tropical Atlantic index (NTAI) is defined by the areal mean SST over the region within 0°–15°N and 90°W–20°E (Figure 8). To investigate the influence of NTA SST on the WPWP SSTs, regressions of tropical climate variables on the preceding August NTAI are calculated. Considering that the interannual variability of NTA SSTs and WPWP SSTs are influenced by the ENSO (Alexander and Scott, 2002; Chiang and Sobel, 2002), the ENSO signal of previous December–February is first removed from the corresponding data before the lagged regression is performed. The ENSO signal is represented using the Niño3.4 index (5°S–5°N, 170°–120°W). Figure 8 shows the seasonal SST anomalies and 850-hPa wind anomalies during autumn, winter, and spring regressed on the detrended and standardized time series of NTAI for August.

During the boreal summer and the early autumn (August–September–October), warm SST anomalies in the NTA area may induce strengthened convective

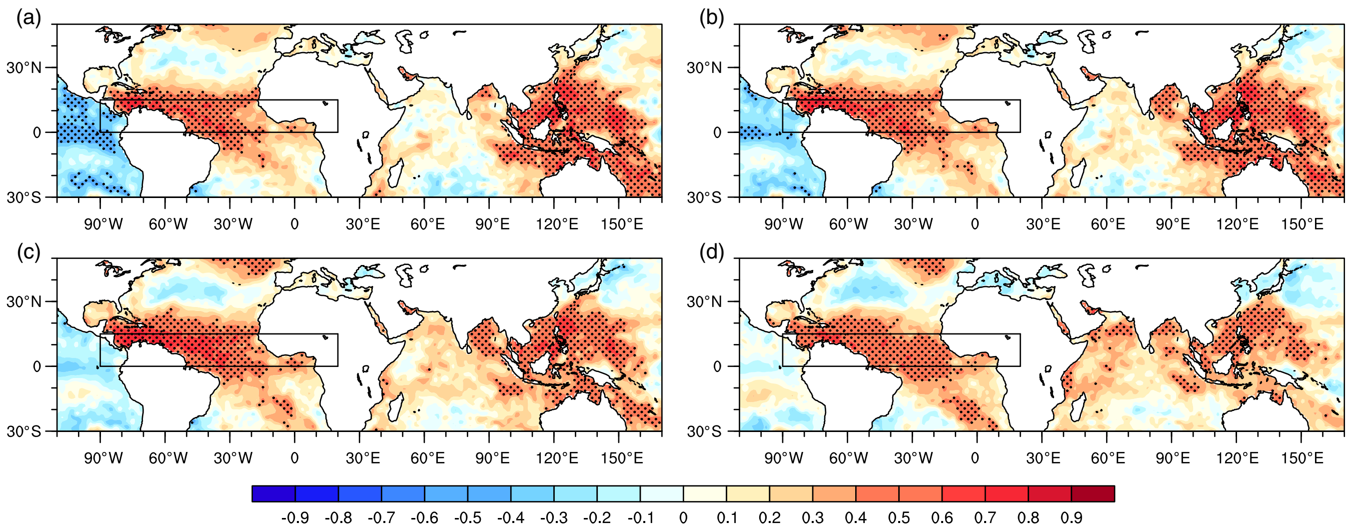

FIGURE 8 Correlation coefficients between observed DY of SST of previous August and observed DY of SST of current year during (a) January, (b) February, (c) March and (d) April. Dotted areas indicate statistical significance at the 99% confidence level based on the Student's *t*-test. The black curvilinear rectangles represent the region of NTA

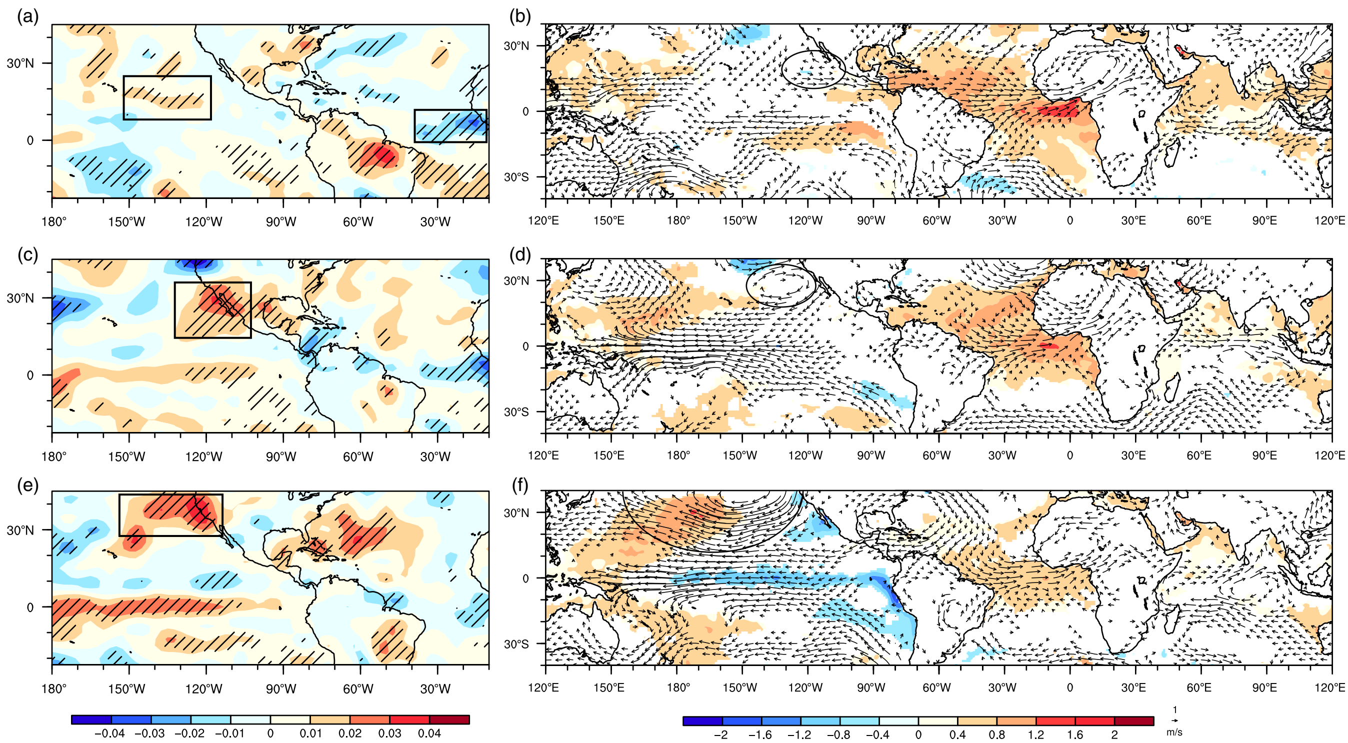

FIGURE 9 Anomalies of observed 850-hPa ω (unit: 10^{-3} Pa s^{-1}; left panel) and SST (unit: °C, colour shading), 850-hPa wind (unit: m s^{-1}, vector; right panel) during (a–b) August–October (the ASO season), (c–d) NDJ and (e–f) FMA of next year regressed on the observed august NTAI for 1961–2006. Slashed areas in (a, c, e) indicate statistical significance at the 90% confidence level based on the Student's *t*-test. As for the 850-hPa wind in (b, d, f), only the values above 0.2 m s^{-1} are shown. As for the SST in (b, d, f), only the values at the 90% confidence level or higher are shown

activity over the subtropical Atlantic within 40°–5°W (Figure 9a), and the associated convective heating may stimulate a Gill-type Rossby wave response characterized by an anomalous low-level cyclone over the subtropical eastern Pacific (Gill, 1980; Figure 9b). The northerly wind anomalies on the west edge of this anomalous cyclone increase the surface wind speed over the subtropical Pacific within 160°–125°W (Figure 10a) and lead to

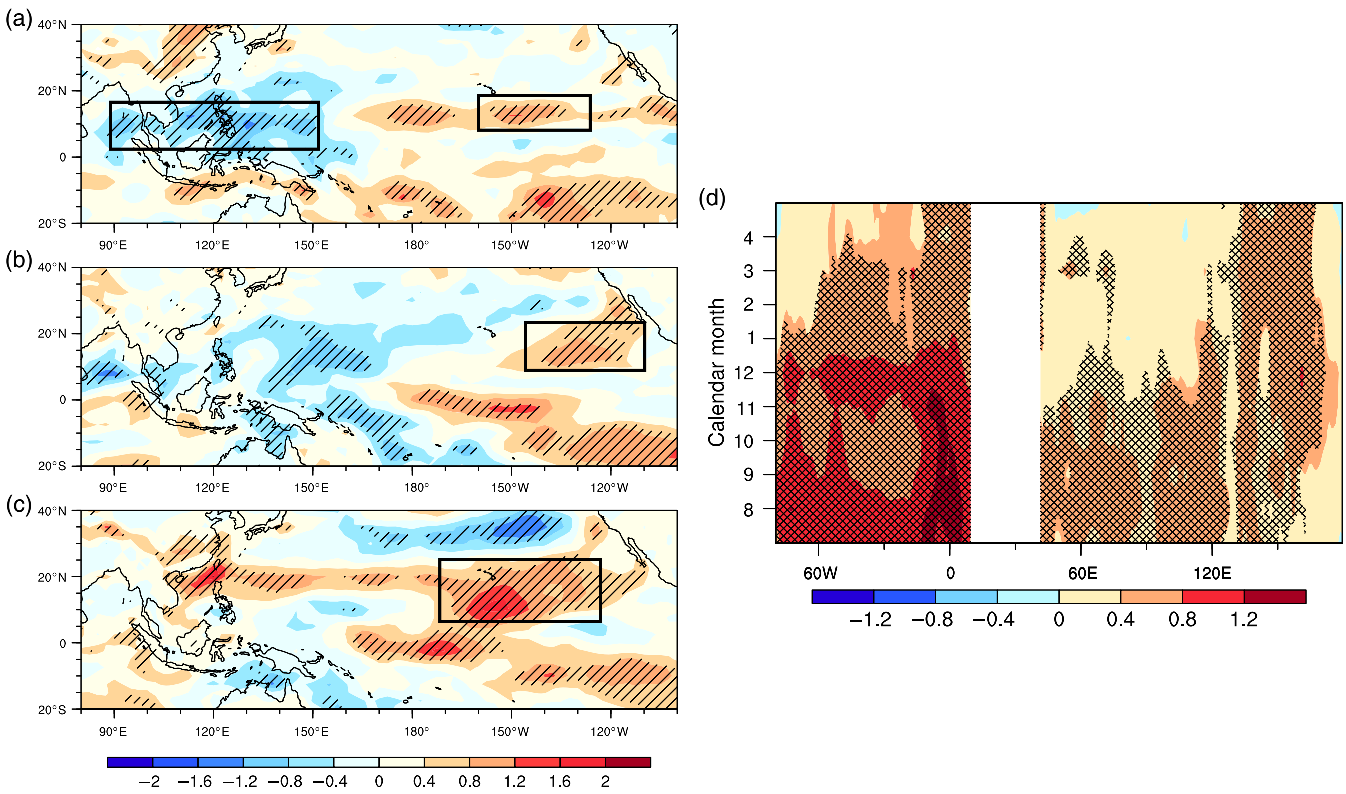

FIGURE 10 Observed surface wind speed (unit: m s^{-1}) during (a) ASO, (b) NDJ, (c) FMA of next year and (d) time–longitude section of observed meridional SST averaged within 0°–15°N (unit: °C) regressed on the observed August NTAI for 1961–2006. Slashed areas in (a–c) indicate statistical significance at the 90% confidence level based on the Student's *t*-test. Crossed areas in (d) indicate statistical significance at the 95% confidence level based on the Student's *t*-test

increased evaporative cooling of the SSTs in this region (Ham *et al*., 2007), which provides an unfavourable condition for the overlaying atmospheric convection and results in weakened convective heating over the subtropical eastern Pacific within 130°–100°W (Figure 9c). The weakened convective heating over the subtropical eastern Pacific may stimulate an anomalous low-level anticyclone over the subtropical central Pacific (Gill, 1980; Figure 9d); in turn, the northerly wind anomalies along the eastern edge of this anomalous anticyclone lead to increased wind speed over the eastern North Pacific within 145°–110°W (Figure 10b), which may further contribute to increased evaporative cooling in the eastern North Pacific (Figure 9f) and hence further lead to weakened convective heating over the eastern North Pacific (Figure 9e). The above positive feedback may eventually result in an anomalous anticyclone occupying North Pacific during winter and the subsequent spring, which induces enhanced low-level easterly winds over the subtropical and tropical Pacific (Figure 9f). These enhanced low-level easterlies over the tropical Pacific would lead to warm SST anomalies in the western tropical Pacific and cold SST anomalies in the central and eastern tropical Pacific (Figure 9f).

In addition to the aforementioned mechanism mediating the influence of NTA SSTs on the WPWP SSTs, there may be another mechanism of preceding August NTA SSTs affecting the January–April WPWP SSTs. As shown in Figure 9b, an anomalous warming in the tropical Atlantic is generally concurrent with an anomalous warming in the northern Indian Ocean during August (Kucharski *et al*., 2008; Wang *et al*., 2009). It has been well known that an anomalous warming in the tropical Atlantic during boreal summer may stimulate an equatorial Kelvin wave which propagates eastward to the Indian Ocean and western tropical Pacific within 2 weeks (Ham *et al*., 2013; Li *et al*., 2016), the Kelvin wave is characterized by easterly low-level wind anomalies over the Indo-Pacific region (Figure 9b). These easterly wind anomalies over the Indo-Pacific region may induce decreased surface wind speed over the tropical Indo-Pacific region within 90°–150°E (Figure 10a), which lead to decreased evaporative cooling of SSTs in this region and hence warm SST anomalies in this region (Xie and Philander, 1994; Figure 9b). The warm SST anomalies in the Indo-Pacific region may in turn induce a secondary circulation during the subsequent NDJ, which results in westerly low-level wind anomalies over the tropical

Indian Ocean and easterly low-level wind anomalies over the western tropical Pacific (Figure 9d). The easterly low-level wind anomalies over western tropical Pacific may enhance the Walker circulation and lead to warm SST anomalies in the WPWP via the Bjerknes feedback (Bjerknes, 1969; Figure 9d), which may persist through the subsequent FMA (Figure 9f). Figure 9d shows regression of subtropical (0°–15°N) SST on the preceding August NTAI, which indicates that the signal of Atlantic-induced warm SST anomalies in the Indian Ocean during preceding August may propagate eastward with time and lead to warm SST anomalies in the western tropical Pacific during the subsequent January–April.

Thus, anomalous warm SSTs in the NTA during the preceding August may contribute to warm WPWP SST anomalies during January–April via two different mechanisms, whereby the observed NTAI during the preceding August can be used as a predictor for establishing the PE model predicting the WPWP SST anomalies.

4.2 | Establishing PE model and improving the numerical model prediction

Based on the above results, two predictors for the PE model predicting the DY_WPWPI during January–April are determined, which are the DY of ENSEMBLES-MME-forecasted SLPI during January (hereafter referred as DY_SLPI) and the DY of observed NTAI during preceding August (hereafter referred as DY_NTAI). The CC between the time series of DY_SLPI and DY_NTAI during 1960–2006 is −0.09, which is below the 90% confidence level, indicating that the two factors are independent. Based on the above two predictors, a PE model is established using a multivariable regression method:

$$\mathrm{DY\_WPWPI} = a \times \mathrm{DY\_SLPI} + b \times \mathrm{DY\_NTAI}$$

where the DY_WPWPI is the monthly DY_WPWPI during January–April; the DY_SLPI is the DY of ENSEMBLES-MME-predicted SLPI during January; the DY_NTAI is the DY of observed NTAI during preceding August; the a and b are the corresponding regression coefficients for DY_SLPI and DY_NTAI, respectively.

Table 1 shows the CCs between the predictors and the predictand. The predictors are significantly correlated with the predictand during January–April, where the corresponding CCs are all at the 99% significance level. Specifically, the CCs between the DY_SLPI during January and the monthly DY_WPWPI during January–April are characterized by negative values smaller than −0.4; the CCs between the monthly DY_NTAI during preceding August and the monthly DY_WPWPI during January–April are characterized by positive values larger than +0.4.

The performance of the PE model is evaluated using a cross-validation method with a one-year-out approach for the period 1963–2006 (44 years) and is also evaluated using independent hindcast for 1985–2006 (22 years).

According to the 1-year-out cross-validation results (Table 2), the CCs between the PE-model-predicted DY_WPWPI and the observed DY_WPWPI are larger than 0.8 for January–March and is approximately 0.7 for April, which are significant at the 99% confidence level. Furthermore, the CCs between the observation and the PE model for the WPWPI are larger than 0.65 for January–April, which are above the 99% significance level. In contrast, the CCs between the ENSEMBLES-MME-predicted DY_WPWPI and the observed DY_WPWPI during January–April are approximately 0.05 (significant below the 90% confidence level), and the CCs between the observation and the ENSEMBLES MME for the WPWPI are approximately 0.15 (significant

TABLE 1 Correlation coefficients between predictors and the predictand (DY_WPWPI) for the period 1960–2006

	Predictors	
Predictand	**DY_SLPI**	**DY_NTAI**
JAN	−0.81	0.47
FEB	−0.77	0.54
MAR	−0.66	0.62
APR	−0.48	0.59

TABLE 2 Correlation coefficients between the PE model and the observation for the WPWPI and DY_WPWPI in cross-validation for the period 1963–2006 and independent hindcast for the period 1985–2006 (CCs between the ENSEMBLES MME and the observation for the WPWPI and DY_WPWPI are in parentheses)

	Cross-validation		Hindcast	
Predictand	**DY_WPWPI**	**WPWPI**	**DY_WPWPI**	**WPWPI**
JAN	0.88 (0.05)	0.72 (0.19)	0.90	0.81
FEB	0.89 (0.05)	0.68 (0.19)	0.92	0.77
MAR	0.85 (0.05)	0.73 (0.19)	0.85	0.75
APR	0.69 (0.05)	0.66 (0.17)	0.74	0.68

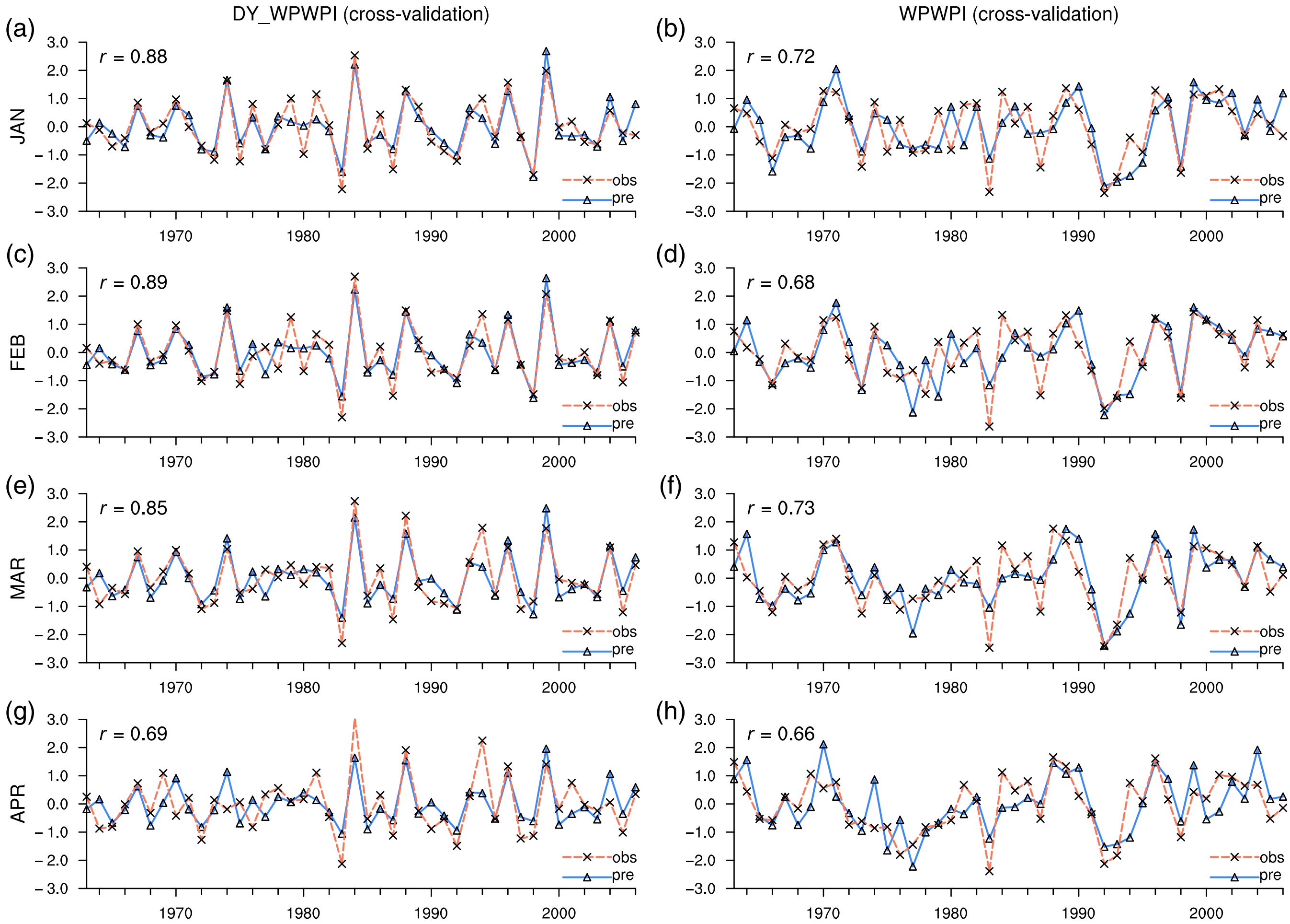

FIGURE 11 The PE-model-predicted (blue line) and observed (orange line) DY_WPWPI (left panel) and WPWPI (right panel) during (a) January, (b) February, (c) March and (d) April in the cross-validation test for the period 1963–2006

below the 90% confidence level). The results of 2/3 years out cross-validation are similar to the result of 1-year-out cross-validation. The above results suggest a good capability of the PE model for improving the WPWP SST prediction of numerical model. Specifically, Figure 11 shows the cross-validation results for DY_WPWPI and WPWPI during January–April. The PE-model-forecasted DY_WPWPIs during January–April are significantly correlated with the observed DY_WPWPIs in the one-year-out cross-validation for the period 1963–2006, with CCs above 0.65 (Figures 11a,c,e,g). Correspondingly, the time series of the PE-model-forecasted WPWPI are also largely consistent with the time series of the observed WPWPIs during January–April regarding the interannual variability (Figures 11b,d,f,h).

As for the independent hindcast for 1985–2006, the CCs between the observation and the PE model for the DY_WPWPI are larger than 0.85 for January–March and is 0.74 for April, which are significant at the 99% confidence level; the CCs between the PE-model-predicted WPWPI and the observed WPWPI during January–April are larger than 0.65, which are also significant at the 99% confidence level (Table 2). Specially, Figure 12 shows the independent hindcast of DY_WPWPI and WPWPI during January–April for 1985–2006 (Figures 12a,c,e,g). The time series of PE-model-forecasted WPWPI and observed WPWPI show similar features (Figures 12b,d,f,h). Thus, the PE model performs well for improving the ENSEMBLES-MME-predicted DY_WPWPIs as well as WPWPIs for January–April.

5 | DISCUSSION AND CONCLUSION

In this study, the predictive ability of the ENSEMBLES MME for the WPWP SST during 1960–2005 is assessed. A relatively poor forecast skill of the ENSEMBLES MME for the WPWPI during January–April is detected, with an insignificant correlation between the ENSEMBLES-

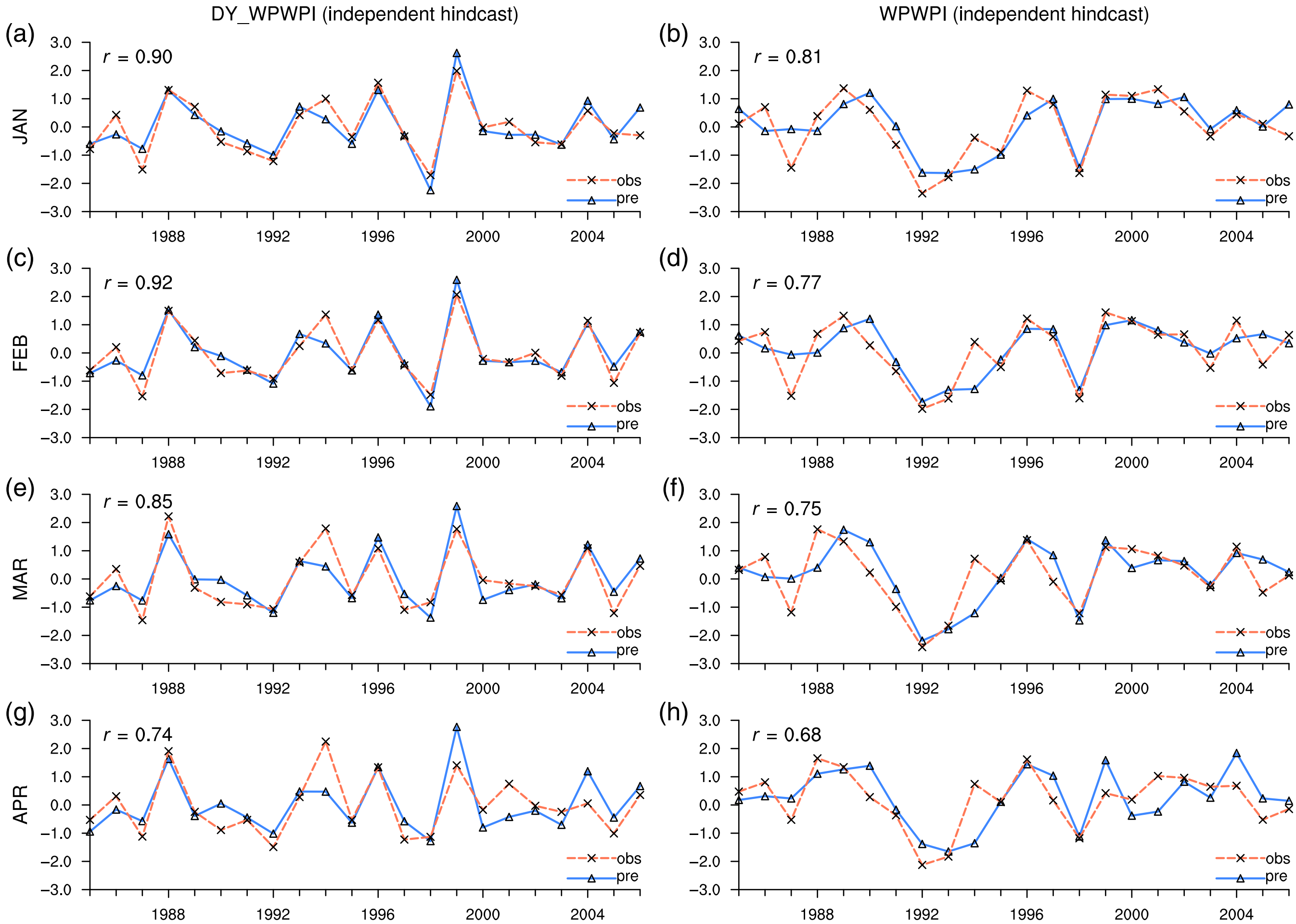

FIGURE 12 The PE-model-predicted (blue line) and observed (orange line) DY_WPWPI (left panel) and WPWPI (right panel) during (a) January, (b) February, (c) March and (d) April in the independent hindcast for the period 1985–2006

MME-predicted WPWPI/DY_WPWPI and the observed WPWPI/ DY_WPWPI during January–April for the period 1960–2005. To improve the prediction of ENSEMBLES MME for the WPWPI during January–April, a PE model is established using the year-to-year increment approach based on two predictors. The two predictors include the ENSEMBLES-MME-predicted SLP during January over the WPWP region and the observed SST in preceding August in the NTA region. The 1-year-out cross-validation and independent hindcast results indicate that the PE model can notably improve the ENSEMBLES-MME-predicted DY_WPWPI as well as WPWPI, suggesting that this PE model may be utilized to improve the numerical-model-predicted WPWP SSTs.

The results of this study suggest that the SLP over the WPWP during January and the NTA SSTs during the preceding August may exert a persistent influence on the WPWP SSTs during January–April via different mechanisms. In addition to those two factors, there are some other factors that may also influence the variability of WPWP SSTs, such as the Niño4 SST during previous year (Fan *et al.*, 2017), the heat flux at the ocean surface in the western Pacific (Wang and Xie, 1998), the Pacific Decadal Oscillation (PDO) during pervious winter (Gan and Wu, 2012). These factors may also be considered to improve the seasonal and interannual forecast of WPWP SSTs in the future.

Finally, this study only focus on improving the prediction of ENSEMBLES MME, there are more recent databases of seasonal forecasts such as CFSv2, Met Office Global Seasonal Forecast System 5 (GloSea5) and EUROpean Seasonal to Interannual Prediction (EUROSIP). Further studies on evaluating and improving the prediction of these numerical model's production are needed.

ACKNOWLEDGEMENTS

This study is funded by the Natural Science Foundation of China (Grants 41805047 and 41421004), the Jiangsu Innovation and Entrepreneurship Team and the Scientific Research Foundation of Key Laboratory of

Meteorological Disaster (KLME), Ministry of Education (KLME201803), the Science and Technology Innovation Project for Overseas Talents of Nanjing (Grant No. R2018LZ02).

ORCID

Ping Chen https://orcid.org/0000-0002-9572-2895

REFERENCES

Alexander, M. and Scott, J. (2002) The influence of ENSO on air-sea interaction in the Atlantic. *Geophysical Research Letters*, 29, 46-1–46-4. https://doi.org/10.1029/2001gl014347.

Berliner, L.M., Wikle, C.K. and Cressie, N. (2000) Long-lead prediction of Pacific SSTs via Bayesian dynamic modeling. *Journal of Climate*, 13, 3953–3968. https://doi.org/10.1175/1520-0442(2001)013<3953:LLPOPS>2.0.CO;2.

Bi, S.T., Wang, P.F., Pan, X.N. and Li, C.F. (2018) Understanding the dynamical mechanism of year-to-year incremental prediction by nonlinear time series prediction theory. *Atmospheric and Oceanic Science Letters*, 11, 71–77. https://doi.org/10.1080/16742834.2017.1345278.

Bjerknes, J. (1969) Atmospheric teleconnection from the equatorial Pacific. *Monthly Weather Review*, 97, 163–172. https://doi.org/10.1175/1520-0493(1969)097<0163:ATFTEP>2.3.CO;2.

Chen, G., Fang, C.Y., Zhang, C.Y. and Chen, Y. (2004) Observing the coupling effect between warm pool and “rain pool” in the Pacific Ocean. *Remote Sensing of Environment*, 91, 153–159. https://doi.org/10.1016/j.rse.2004.02.010.

Chiang, J.C.H. and Sobel, A.H. (2002) Tropical tropospheric temperature variations caused by ENSO and their influence on the remote tropical climate. *Journal of Climate*, 15, 2616–2631. https://doi.org/10.1175/1520-0442(2002)015<2616:TTTVCB>2.0.CO;2.

Clement, A.C., Seager, R. and Murtugudde, R. (2005) Why are there tropical warm pools? *Journal of Climate*, 18, 5294–5311. https://doi.org/10.1175/JCLI3582.1.

Cronin, M.F. and McPhaden, M.J. (1997) The upper ocean heat balance in the western equatorial Pacific warm pool during september–december 1992. *Journal of Geophysical Research*, 102, 8533–8553. https://doi.org/10.1029/97JC00020.

D'Arrigo, R., Wilson, R., Palmer, J., Krusic, P., Curtis, A., Sakulich, J., Bijaksana, S., Zulaikah, S., Ngkoimani, L.O. and Tudhope, A. (2006) The reconstructed Indonesian warm pool sea surface temperatures from tree rings and corals: linkages to Asian monsoon drought and El Niño-southern oscillation. *Paleoceanography*, 21, 1–13. https://doi.org/10.1029/2005PA001256.

Da Silva, A.M., Young, C.C. and Levitus, S. (1994) *Algorithms and procedures. Vol. 1, Atlas of surface marine data 1994*. Washington, DC: U. S. Department of Commerce, National Oceanic and Atmospheric Administration, p. 83.

De Deckker, P. (2016) The Indo-Pacific warm pool: critical to world oceanography and world climate. *Geoscience Letters*, 3, 20. https://doi.org/10.1186/s40562-016-0054-3.

Doblas-Reyes, F.J., Weisheimer, A., Déqué, M., Keenlyside, N., McVean, M., Murphy, J.M., Rogel, P., Smith, D. and Palmer, T. N. (2009) Addressing model uncertainty in seasonal and annual dynamical ensemble forecasts. *Quarterly Journal of the Royal Meteorological Society*, 135, 1538–1559. https://doi.org/10.1002/qj.464.

Druyan, L.M. and Hastenrath, S. (2002) Tropical impacts of SST forcing: a case study for 1987 versus 1988. *Journal of Climate*, 7, 1316–1323. https://doi.org/10.1175/1520-0442(1994)007<1316:tiosfa>2.0.co;2.

Enfield, D.B., Lee, S.K. and Wang, C.Z. (2006) How are large western hemisphere warm pools formed? *Progress in Oceanography*, 70, 346–365. https://doi.org/10.1016/j.pocean.2005.07.006.

Fan, K., Wang, H.J. and Choi, Y.J. (2008) A physically-based statistical forecast model for the middle-lower reaches of the Yangtze River valley summer rainfall. *Chinese Science Bulletin*, 53, 602–609. https://doi.org/10.1007/s11434-008-0083-1.

Fan, K., Tian, B.Q. and Wang, H.J. (2016) New approaches for the skillful prediction of the winter North Atlantic oscillation based on coupled dynamic climate models. *International Journal of Climatology*, 36, 82–94. https://doi.org/10.1002/joc.4330.

Fan, J., Hu, D.X., Hu, S.J. and Feng, J.Q. (2017) Niño4 as a key region for the interannual variability of the Western Pacific warm pool. *Journal of Geophysical Research, Oceans*, 122, 9299–9314. https://doi.org/10.1002/2017JC013208.

Frauen, C. and Dommenget, D. (2012) Influences of the tropical Indian and Atlantic oceans on the predictability of ENSO. *Geophysical Research Letters*, 39, 2–7. https://doi.org/10.1029/2011GL050520.

Gan, B.L. and Wu, L.X. (2012) Possible origins of the Western pacific warm pool decadal variability. *Advances in Atmospheric Sciences*, 29, 169–176. https://doi.org/10.1007/s00376-011-0193-6.

Gao, X.J. and Giorgi, F. (2017) Use of the RegCM system over East Asia: review and perspectives. *Engineering*, 3, 766–772. https://doi.org/10.1016/J.ENG.2017.05.019.

Gao, X.J., Luo, Y., Lin, W.T., Zhao, Z.C. and Giorgi, F. (2008) Simulation of effects of land use change on climate in China by a regional climate model. *Advances in Atmospheric Sciences*, 20, 583–592. https://doi.org/10.1007/bf02915501.

Gao, X.J., Wu, J., Shi, Y., Wu, J., Han, Z.Y., Zhang, D.F., Tong, Y., Li, R.K., Xu, Y. and Giorgi, F. (2018) Future changes in thermal comfort conditions over China based on multi-RegCM4 simulations. *Atmospheric and Oceanic Science Letters*, 11, 291–299. https://doi.org/10.1080/16742834.2018.1471578.

Gill, A.E. (1980) Some simple solutions for heat-induced tropical circulation. *Quarterly Journal of the Royal Meteorological Society*, 106, 447–462.

Graham, N.E., Michaelsen, J. and Barnett, T.P. (1987) An investigation of the El Niño-southern oscillation cycle with statistical models: 2. Model results. *Journal of Geophysical Research*, 92, 14271. https://doi.org/10.1029/JC092iC13p14271.

Ham, Y.G., Kug, J.S. and Kang, I.S. (2007) Role of moist energy advection in formulating anomalous Walker circulation associated with El Niño. *Journal of Geophysical Research – Atmospheres*, 112, 1–10. https://doi.org/10.1029/2007JD008744.

Ham, Y.G., Kug, J.S., Park, J.Y. and Jin, F.F. (2013) Sea surface temperature in the north tropical Atlantic as a trigger for El Niño/southern oscillation events. *Nature Geoscience*, 6, 112–116. https://doi.org/10.1038/ngeo1686.

Hu, S.J., Hu, D.X., Guan, C., Xing, N., Li, J.P. and Feng, J.Q. (2017) Variability of the Western Pacific warm pool structure associated with El Niño. *Climate Dynamics*, 49, 2431–2449. https://doi.org/10.1007/s00382-016-3459-y.

Huang, R.H. (1992) The East Asia/Pacific pattern teleconnection of summer circulation and climate anomaly in East Asia. *Acta Meteorologica Sinica*, 6, 25–37.

Huang, Y.Y., Wang, H.J. and Fan, K. (2014) Improving the prediction of the summer Asian–Pacific oscillation using the interannual increment approach. *Journal of Climate*, 27, 8126–8134. https://doi.org/10.1175/JCLI-D-14-00209.1.

Huo, W.J. and Xiao, Z.N. (2017) Anomalous pattern of ocean heat content during different phases of the solar cycle in the tropical Pacific. *Atmospheric and Oceanic Science Letters*, 10, 9–16. https://doi.org/10.1080/16742834.2017.1247412.

Jansen, M.F., Dommenget, D. and Keenlyside, N. (2009) Tropical atmosphere-ocean interactions in a conceptual framework. *Journal of Climate*, 22, 550–567. https://doi.org/10.1175/2008JCLI2243.1.

Kalnay, E., Kanamitsu, M., Kistler, R., Collins, W., Deaven, D., Gandin, L., Iredell, M., Saha, S., White, G., Woollen, J., Zhu, Y., Leetmaa, A., Reynolds, R., Chelliah, M., Ebisuzaki, W., Higgins, W., Janowiak, J., Mo, K.C., Ropelewski, C., Wang, J., Jenne, R. and Joseph, D. (1996) The NCEP/NCAR 40-year reanalysis project. *Bulletin of the American Meteorological Society*, 77, 437–471. https://doi.org/10.1175/1520-0477(1996)077<0437:TNYRP>2.0.CO;2.

Kang, I.S. and Kug, J.S. (2000) An El-Nino prediction system using an intermediate ocean and a statistical atmosphere. *Geophysical Research Letters*, 27, 1167–1170. https://doi.org/10.1029/1999GL011023.

Kitoh, A., Motoi, T. and Koide, H. (1999) SST variability and its mechanism in a coupled atmosphere-mixed layer ocean model. *Journal of Climate*, 12, 1221–1239. https://doi.org/10.1175/1520-0442(1999)012<1221:SVAIMI>2.0.CO;2.

Knaff, J.A. (1997) Implications of summertime sea level pressure anomalies in the tropical Atlantic region. *Journal of Climate*, 10, 789–804. https://doi.org/10.1175/1520-0442(1997)010<0789:IOSSLP>2.0.CO;2.

Koh, T.Y. and Ng, J.S. (2009) Improved diagnostics for NWP verification in the tropics. *Journal of Geophysical Research – Atmospheres*, 114, 1–13. https://doi.org/10.1029/2008JD011179.

Kucharski, F., Bracco, A., Yoo, J.H. and Molteni, F. (2008) Atlantic forced component of the Indian monsoon interannual variability. *Geophysical Research Letters*, 35, 1–5. https://doi.org/10.1029/2007GL033037.

Kucharski, F., Kang, I.S., Farneti, R. and Feudale, L. (2011) Tropical Pacific response to 20th century Atlantic warming. *Geophysical Research Letters*, 38, 1–5. https://doi.org/10.1029/2010GL046248.

Kucharski, F., Parvin, A., Rodriguez-fonseca, B., Farneti, R., Martin-Rey, M., Polo, I., Mohino, E., Losada, T. and Mechoso, R. C. (2016) The teleconnection of the tropical Atlantic to Indo-Pacific sea surface temperatures on inter-annual to centennial time dcales: A review of recent findings. *Atmosphere*, 7, 1–20. https://doi.org/10.3390/atmos7020029.

Li, W.B. and Zhou, C.P. (1999) The impacts of tropical Western Pacific warm pool on precipitation and disasters in coastal region of China. *Acta Scicentiarum Naturalum*, 35, 674–681. https://doi.org/10.13209/j.0479-8023.1999.099.

Li, D.H., Zhu, Y.M., Tan, Y.K. and Zhang, G. (2006) Relationships between Spring Ocean sea surface temperature anomalies in the tropical Indian Ocean and the strength of South China Sea summer monsoon. *Climatic and Environmental Research*, 11, 514–524. http://doi.org/10.3969/j.issn.1006-9585.2006.04.008.

Li, X.C., Xie, S.P., Gille, S.T. and Yoo, C.H. (2016) Atlantic-induced pan-tropical climate change over the past three decades. *Nature Climate Change*, 6, 275–279. https://doi.org/10.1038/nclimate2840.

Li, H.X., Chen, H.P. and Wang, H.J. (2017) Influence of North Pacific SST on heavy precipitation events in autumn over North China. *Atmospheric and Oceanic Science Letters*, 10, 21–28. https://doi.org/10.1080/16742834.2017.1237256.

Luksch, U. and von Storch, H. (1992) Modeling the low-frequency sea surface temperature variability in the North Pacific. *Journal of Climate*, 5, 893–906. https://doi.org/10.1175/1520-0442(1992)005<0893:MTLFSS>2.0.CO;2.

Madden, R.A. and Julian, P.R. (1994) Observations of the 40–50-day tropical oscillation—a review. *Monthly Weather Review*, 122, 814–837. https://doi.org/10.1175/1520-0493(1994)122<0814:OOTDTO>2.0.CO;2.

Matsuura, T. and Iizuka, S. (2000) Zonal migration of the Pacific warm-pool tongue during El Niño events. *Journal of Physical Oceanography*, 30, 1582–1600. https://doi.org/10.1175/1520-0485(2000)030<1582:ZMOTPW>2.0.CO;2.

Michaelsen, J. (1987) Cross-validation in statistical climate forecast models. *Journal of Climate and Applied Meteorology*, 26, 1589–1600. https://doi.org/10.1175/1520-0450(1987)026<1589:CVISCF>2.0.CO;2.

Nitta, T. (1986) Long-term variations of cloud amount in the western Pacific region. *Journal of the Meteorological Society of Japan Series II*, 64, 373–390. https://doi.org/10.2151/jmsj1965.64.3_373.

Nitta, T. (1987) Convective activities in the tropical Western Pacific and their impact on the northern hemisphere summer circulation. *Journal of the Meteorological Society of Japan Series II*, 65, 373–390. https://doi.org/10.2151/jmsj1965.65.3_373.

Picaut, J., Loualalen, M., Menkes, C., Delcroix, T. and McPhaden, M.J. (1996) Mechanism of the zonal displacements of the Pacific warm pool: implications for ENSO. *Science*, 274, 1486–1489. https://doi.org/10.1126/science.274.5292.1486.

Rajeevan, M. and McPhaden, M.J. (2004) Tropical Pacific upper ocean heat content variations and Indian summer monsoon rainfall. *Geophysical Research Letters*, 31, 1–4. https://doi.org/10.1029/2004GL020631.

Rayner, N.A., Parker, D.E., Horton, E.B., Folland, C.K., Alexander, L.V., Rowell, D.P., Kent, E.C. and Kaplan, A. (2003) Global analyses of sea surface temperature, sea ice, and night marine air temperature since the late nineteenth century. *Journal of Geophysical Research*, 108, 4407. https://doi.org/10.1029/2002JD002670.

Ridout, J.A. and Reynolds, C.A. (1998) Western Pacific warm pool region sensitivity to convective triggering by boundary layer thermals in the NOGAPS atmospheric GCM. *Journal of Climate*, 11, 1553–1573. https://doi.org/10.1175/1520-0442(1998)011<1553:WPWPRS>2.0.CO;2.

Ruiz, J.E., Cordery, I. and Sharma, A. (2005) Integrating Ocean subsurface temperatures in statistical ENSO forecasts. *Journal of Climate*, 18, 3571–3586. https://doi.org/10.1175/JCLI3477.1.

Saha, S., Nadiga, S., Thiaw, C., Wang, J., Wang, W., Zhang, Q., Van den Dool, H.M., Pan, H.L., Moorthi, S., Behringer, D., Stokes, D., Peña, M., Lord, S., White, G., Ebisuzaki, W., Peng, P. and Xie, P. (2006) The NCEP climate forecast system. *Journal of Climate*, 19, 3483–3517. https://doi.org/10.1175/JCLI3812.1.

Shen, H.B., He, S.P. and Wang, H.J. (2019) Effect of summer Arctic Sea ice on the reverse august precipitation anomaly in eastern China between 1998 and 2016. *Journal of Climate*, 32, 3389–3407. https://doi.org/10.1175/JCLI-D-17-0615.1.

Shinoda, T. and Hendon, H.H. (1998) Mixed layer modeling of intraseasonal variability in the tropical western Pacific and Indian oceans. *Journal of Climate*, 11, 2668–2685. https://doi.org/10.1175/1520-0442(1998)011<2668:MLMOIV>2.0.CO;2.

Soden, B.J. and Vecchi, G.A. (2011) The vertical distribution of cloud feedback in coupled ocean-atmosphere models. *Geophysical Research Letters*, 38, 1–6. https://doi.org/10.1029/2011GL047632.

Stockdale, T.N., Anderson, D.L.T., Balmaseda, M.A., Doblas-Reyes, F., Ferranti, L., Mogensen, K., Palmer, T.N., Molteni, F. and Vitart, F. (2011) ECMWF seasonal forecast system 3 and its prediction of sea surface temperature. *Climate Dynamics*, 37, 455–471. https://doi.org/10.1007/s00382-010-0947-3.

Sun, J.Q., Wu, S. and Ao, J. (2016) Role of the north Pacific Sea surface temperature in the east Asian winter monsoon decadal variability. *Climate Dynamics*, 46, 3793–3805. https://doi.org/10.1007/s00382-015-2805-9.

Sun, C., Kucharski, F., Li, J.P., Jin, F.F., Kang, I.S. and Ding, R.Q. (2017) Western tropical Pacific multidecadal variability forced by the Atlantic multidecadal oscillation. *Nature Communications*, 8, 1–10. https://doi.org/10.1038/ncomms15998.

Sun, Q., Wu, B., Zhou, T.J. and Yan, Z.X. (2018) ENSO hindcast skill of the IAP-DecPreS near-term climate prediction system: comparison of full-field and anomaly initialization. *Atmospheric and Oceanic Science Letters*, 11, 54–62. https://doi.org/10.1080/16742834.2018.1411753.

Tangang, F.T., Hsieh, W.W. and Tang, B. (1997) Forecasting the equatorial Pacific Sea surface temperatures by neural network models. *Climate Dynamics*, 13, 135–147. https://doi.org/10.1007/s003820050156.

Tian, B.Q. and Fan, K. (2014) A skillful prediction model for winter NAO based on Atlantic Sea surface temperature and Eurasian snow cover. *Weather and Forecasting*, 30, 197–205. https://doi.org/10.1175/waf-d-14-00100.1.

Tian, B.Q., Fan, K. and Yang, H.Q. (2018) East Asian winter monsoon forecasting schemes based on the NCEP's climate forecast system. *Climate Dynamics*, 51, 2793–2805. https://doi.org/10.1007/s00382-017-4045-7.

Timmermann, A., Okumura, Y., An, S.I., Clement, A., Dong, B., Guilyardi, E., Hu, A., Jungclaus, J.H., Renold, M., Stocker, T.F., Stouffer, R.J., Sutton, R., Xie, S.P. and Yin, J. (2007) The influence of a weakening of the Atlantic meridional overturning circulation on ENSO. *Journal of Climate*, 20, 4899–4919. https://doi.org/10.1175/JCLI4283.1.

Wang, C.Z. and Enfield, D.B. (2001) The tropical Western hemisphere warm pool. *Geophysical Research Letters*, 28, 1635–1638. https://doi.org/10.1029/2000GL011763.

Wang, H. and Mehta, V.M. (2008) Decadal variability of the Indo-Pacific warm pool and its association with atmospheric and oceanic variability in the NCEP-NCAR and SODA reanalyses. *Journal of Climate*, 21, 5545–5565. https://doi.org/10.1175/2008JCLI2049.1.

Wang, B. and Xie, X.S. (1998) Coupled modes of the warm pool climate system. Part I: the role of air-sea interaction in maintaining Madden-Julian oscillation. *Journal of Climate*, 11, 2116–2135. https://doi.org/10.1175/1520-0442(1998)011<2116:CMOTWP>2.0.CO;2.

Wang, H.J., Zhou, G.Q. and Zhao, Y. (2000) An effective method for correcting the seasonal-interannual prediction of summer climate anomaly. *Advances in Atmospheric Sciences*, 17, 234–240. https://doi.org/10.1007/s00376-000-0006-9.

Wang, C.Z., Kucharski, F., Barimalala, R. and Bracco, A. (2009) Teleconnections of the tropical Atlantic to the tropical Indian and Pacific oceans: a review of recent findings. *Meteorologische Zeitschrift*, 18, 445–454. https://doi.org/10.1127/0941-2948/2009/0394.

Wang, W., Chen, M. and Kumar, A. (2010) An assessment of the CFS real-time seasonal forecasts. *Weather and Forecasting*, 25, 950–969. https://doi.org/10.1175/2010WAF2222345.1.

Webster, P.J. and Lukas, R. (1992) TOGA COARE: the coupled ocean-atmosphere response experiment. *Bulletin of the American Meteorological Society*, 73, 1377–1416. https://doi.org/10.1175/1520-0477(1992)073<1377:TCTCOR>2.0.CO;2.

Weisheimer, A., Doblas-Reyes, F.J., Palmer, T.N., Alessandri, A., Arribas, A., Déqué, M., Keenlyside, N., MacVean, M., Navarra, A. and Rogel, P. (2009) ENSEMBLES: a new multi-model ensemble for seasonal-to-annual predictions—skill and progress beyond DEMETER in forecasting tropical Pacific SSTs. *Geophysical Research Letters*, 36, 1–6. https://doi.org/10.1029/2009GL040896.

Wu, Z.M. (1993) Analysis of formation of the equatorial Western Pacific warm pool. *Journal of Ocean University of Qingdao*, S2, 149–152.

Wu, A., Hsieh, W.W. and Tang, B.Y. (2006) Neural network forecasts of the tropical Pacific Sea surface temperatures. *Neural Networks*, 19, 145–154. https://doi.org/10.1016/j.neunet.2006.01.004.

Xie, S.P. and Philander, S.G.H. (1994) A coupled ocean-atmosphere model of relevance to the ITCZ in the eastern Pacific. *Tellus*, 46A, 340–350. https://doi.org/10.1034/j.1600-0870.1994.t01-1-00001.x.

Xue, Y. and Leetmaa, A. (2000) Forecasts of tropical Pacific SST and sea level using a Markov model. *Geophysical Research Letters*, 27, 2701–2704. https://doi.org/10.1029/1999GL011107.

Zelinka, M.D. and Hartmann, D.L. (2010) Why is longwave cloud feedback positive? *Journal of Geophysical Research – Atmospheres*, 115, 1–16. https://doi.org/10.1029/2010JD013817.

Zhan, R.F., Wang, Y.Q. and Wen, M. (2013) The SST gradient between the southwestern Pacific and the western Pacific warm pool: a new factor controlling the northwestern Pacific tropical cyclone genesis frequency. *Journal of Climate*, 26, 2408–2415. https://doi.org/10.1175/JCLI-D-12-00798.1.

Zhang, R. and Delworth, T.L. (2007) Impact of the Atlantic multidecadal oscillation on North Pacific climate variability. *Geophysical Research Letters*, 34, 2–7. https://doi.org/10.1029/2007GL031601.

Zhang, D.P., Huang, Y.Y. and Sun, B. (2019a) Verification and improvement of the capability of ENSEMBLES to predict the winter Arctic oscillation. *Earth and Space Science*, 6, 1887–1899. https://doi.org/10.1029/2019EA000771.

Zhang, D.P., Huang, Y.Y., Sun, B., Li, F. and Wang, H.J. (2019b) Verification and improvement of the ability of CFSv2 to predict the Antarctic oscillation in boreal spring. *Advances in Atmospheric Sciences*, 36, 292–302. https://doi.org/10.1007/s00376-018-8106-6.

How to cite this article: Chen P, Sun B. Improving the dynamical seasonal prediction of western Pacific warm pool sea surface temperatures using a physical–empirical model. *Int J Climatol*. 2020;1–19. https://doi.org/10.1002/joc.6481